

MIT Open Access Articles

Mechanistically Guided Design of Ligands That Significantly Improve the Efficiency of CuH-Catalyzed Hydroamination Reactions

The MIT Faculty has made this article openly available. **Please share** how this access benefits you. Your story matters.

Citation: Thomas, Andy, et al. "Mechanistically Guided Design of Ligands That Significantly Improve the Efficiency of CuH-Catalyzed Hydroamination Reactions." *Journal of the American Chemical Society* 140, 42 (Sept. 2018): p. 13976-84 doi 10.1021/JACS.8B09565 ©2018 Author(s)

As Published: 10.1021/JACS.8B09565

Publisher: American Chemical Society (ACS)

Persistent URL: <https://hdl.handle.net/1721.1/126097>

Version: Author's final manuscript: final author's manuscript post peer review, without publisher's formatting or copy editing

Terms of Use: Article is made available in accordance with the publisher's policy and may be subject to US copyright law. Please refer to the publisher's site for terms of use.





Published in final edited form as:

J Am Chem Soc. 2018 October 24; 140(42): 13976–13984. doi:10.1021/jacs.8b09565.

Mechanistically Guided Design of Ligands that Significantly Improve the Efficiency of CuH-Catalyzed Hydroamination Reactions

Andy A. Thomas^{#1}, Klaus Speck^{#1}, Ilia Kevlishvili^{#2}, Zhaohong Lu¹, Peng Liu², and Stephen L. Buchwald¹

¹Department of Chemistry, Massachusetts Institute of Technology, Cambridge, Massachusetts 02139, United States.

²Department of Chemistry, University of Pittsburgh, Pittsburgh, Pennsylvania 15260, United States.

[#] These authors contributed equally to this work.

Abstract

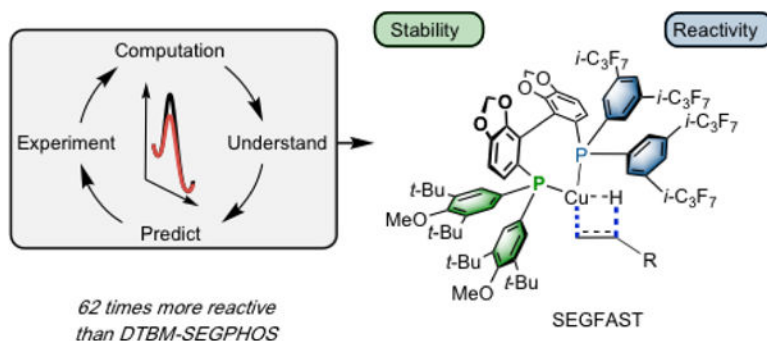
Using a mechanistically guided ligand design approach, a new ligand (SEGFAST) for the CuH-catalyzed hydroamination reaction of unactivated terminal olefins has been developed, providing a 62-fold rate increase over reactions compared to DTBM-SEGPHOS, the previous optimal ligand. Combining the respective strengths of computational chemistry and experimental kinetic measurements, we were able to quickly identify potential modifications that lead to more effective ligands, thus avoiding synthesizing and testing a large library of ligands. By optimizing the combination of attractive, non-covalent ligand-substrate interactions and the stability of the catalyst under the reaction conditions, we were able to identify a finely-tuned hybrid ligand that greatly enables accelerated hydrocupration rates with unactivated alkenes. Moreover, a modular and robust synthetic sequence was devised, which allowed for practical, gram-scale synthesis of these novel hybrid ligand structures.

Graphical Abstract

Address Correspondence to: Professor Stephen L. Buchwald, 18-490 Dreyfus Laboratory, Department of Chemistry, Massachusetts Institute of Technology, 77 Massachusetts Avenue, Cambridge, MA 02139, tel: (617) 253-1885, FAX: (617) 253-3297, slbuchwald@mit.edu.

SUPPORTING INFORMATION

The Supporting Information is available free of charge on the ACS Publications website at DOI: XX. Full computational and experimental procedures along with characterization data and copies of ¹H, ¹³C, ³¹P, and ¹⁹F, spectra, along with full kinetic data are provided.



INTRODUCTION

In 2013, Buchwald,¹ and Miura and Hirano² independently demonstrated that copper hydride complexes (LCuH) can catalyze the chemo- and enantioselective hydroamination reactions between olefins and hydroxylamine esters (Figure 1a). Since then the generality and applicability of this approach has been well demonstrated for a variety of substrates such as styrenes,³ vinylsilanes,⁴ alkynes⁵ and occasionally unactivated olefins,⁶ highlighting its enormous potential. Despite these achievements hydroamination reactions catalyzed by LCuH are not without limitations.⁷ For example, transformation of coupling partners such as cyclic, internal, and some unactivated terminal olefins often require elevated temperatures and increased reaction times compared to those of activated substrates.⁸ In particular, an efficient *anti*-Markovnikov hydroamination reaction with unactivated terminal olefins is highly desirable, because the products of these reactions are frequently found in bioactive molecules.⁹ These compounds are traditionally prepared by transforming carbonyl compounds, amides or alkyl electrophiles into their corresponding amine products.¹⁰ From a strategic standpoint, hydroamination reactions between olefins and electrophilic amine sources provide one of the most straightforward and general avenues to access these important motifs, especially since the precursors are typically stable, readily available, and easy to handle.¹¹

Recently, several experimental^{12,13} and computational¹⁴ mechanistic investigations have appeared on both CuH catalyzed hydroamination and hydroboration reactions, revealing the same basic catalytic cycle, comprised of four elementary steps: hydrocupration (I), oxidative addition (II), reductive elimination (III) and σ -bond metathesis (IV) (Figure 1b).¹⁵ These studies demonstrated that the rate determining step (RDS) can vary between different olefinic substrates. Specifically, the RDS for activated substrates, such as styrenes, is often the catalyst regeneration by σ -bond metathesis, whereas it changes to the hydrocupration step for unactivated internal or terminal alkenes,^{12, 14a} indicating that the lower reactivity observed for unactivated olefins is the direct result of higher barriers for hydrocupration.

Typically, reaction development in this area has relied on empirical observations pertaining to which catalytic system provides the fastest reaction rates.¹¹ For example, reactions with SEGPHOS **L1** supported LCuH catalysts are often found to be slower; whereas, the use of sterically more demanding DTBM-SEGPHOS **L2** derivative is often key to achieving higher reactivity, especially in the reactions of unactivated olefins (Figure 1c).^{14a}

Beginning last year, our laboratories sought to unravel the theoretical foundations that lead to favorable hydrocupration events between LCuH (L = **L1** and **L2**) and various unactivated olefins, by performing the ligand-substrate interaction model analysis on this crucial step (Figure 2a).^{14a} Using this approach, the contributions of the different types of catalyst-substrate interactions to the overall activation energy (E^\ddagger) were split into three categories: (1) the distortion energy required for the LCuH and the substrate to reach their transition state geometries (E_{dist}); (2) the through-space interactions between the ligand and the substrate ($E_{\text{int-space}}$); and (3) the through-bond interactions between the CuH moiety and the substrate ($E_{\text{int-bond}}$). In the hydroamination reactions when SEGPHOS **L1** and DTBM-SEGPHOS **L2** ligands were employed, the E_{dist} and $E_{\text{int-bond}}$ terms were not found to correlate with the overall activation energies (E^\ddagger); however, excellent linear correlations were observed with $E_{\text{int-space}}$. This suggested that the *t*-butyl substituents at the 3- and 5-positions on the *P*-aryl₂ groups in DTBM-SEGPHOS **L2** promote stabilizing non-covalent interactions (Figure 2b). Indeed, dissecting the $E_{\text{int-space}}$ term into its individual components revealed that attractive London dispersion forces (E_{disp}) between the 3,5-di-*t*-butyl substituents on the *P*-aryl₂ groups and the substrate were the main contributing factor to achieve high catalyst activity with the DTBM-SEGPHOS **L2** ligand. While the London dispersion interactions are relatively weak (0.5~1.5 kcal/mol for interactions with each *t*-Bu substituent),^{14a,16} collectively they significantly reduce activation barriers *via* transition state stabilization.^{17,18} Moreover, these conclusions were experimentally validated through ligand synthesis and subsequent kinetic analysis.^{14a}

Building upon this knowledge, we undertook the challenge of designing a new family of ligands based on SEGPHOS **L1** to more efficiently facilitate the copper-hydride catalyzed *anti*-Markovnikov hydroamination reaction with terminal olefins. We theorized a more effective ligand system can be rationally designed by retaining the stabilizing dispersion effects of DTBM-SEGPHOS **L2** while incorporating other types of stabilizing through-bond and/or through-space interactions.¹⁹ Specifically, we surmised that other types of weak non-covalent interactions with the olefin substrate,²⁰ may be harnessed by installation of heteroatom-containing substituents on the *P*-aryl₂ groups. In addition, the through-bond stabilization between the CuH moiety and the substrate in the hydrocupration transition state can be fine-tuned by altering the electronic character of the ligands. However, when designing catalysts capable of promoting reactivity through an assortment of stabilizing interactions, infinite possibilities are conceivable. With the unique ability to computationally quantify and experimentally verify these interactions, an iterative catalyst design approach was envisioned (Figure 3).^{21,22} This approach comprised of four stages: (1) experimentally identify a suitable class of ligand derivatives; (2) using computational analysis to understand what key interactions can stabilize the transition state; (3) using this knowledge to computationally predict a more effective ligand and (4) experimentally test the ligand providing feedback for the next round of ligand optimization.

3.1. Kinetic and computational analysis of SEGPHOS Ligands.

3.1.1. Preliminary Experimental Investigations with Symmetric SEGPHOS Ligands.—As described above, previous investigations indicated that primarily bulky substituents at the 3 and 5-positions on the *P*-aryl₂ groups were critical in facilitating the

hydrocupration event with terminal olefins.^{14a} This finding directed our preliminary studies to investigate SEGPHOS derivatives with substituents possessing different steric (TMS) and electronic (CF₃) properties at these positions (Scheme 1).²³ To kinetically quantify and compare the effects of these ligands on the hydrocupration event 4-phenyl-1-butene (**1**) and *O*-benzoyl-*N,N*-dibenzylhydroxylamine (**2**) were selected as model substrates, because a first order dependence on the olefin had been shown previously for the hydroamination reaction with DTBM-SEGPHOS **L2**.²⁴ The initial rates were measured for the reaction with each ligand by monitoring the formation of hydroamination product **3** under typical copper hydride hydroamination conditions (1.0 mol% Cu(OAc)₂, 1.1 mol% ligand, 0.36 M in THF, 23 °C) utilizing dimethoxydimethylsilane (DMDS, 3.0 equiv/**1**) as the stoichiometric reductant. To allow for a straightforward comparison, the rate of hydroamination was measured first with DTBM-SEGPHOS **L2** ($8.60 \pm 0.05 \times 10^{-6}$ M/s) so that the rates could be normalized (Scheme 1).

Following our standard protocol, the reaction employing TMS-SEGPHOS **L3** was found to be 3.3 times faster than that with DTBM-SEGPHOS **L2**, suggesting that the larger TMS substituents, with a Taft value of $E_s' = 1.79$, have stronger interactions with the olefin substrate than the *t*-Bu groups ($E_s' = 1.49$) in DTBM-SEGPHOS **L2** (Scheme 1).²⁵ Interestingly, the hydroamination with the CF₃-SEGPHOS **L4** derivative underwent the hydrocupration event 6.7 times faster than **L2** and 2.0 times faster than **L3** even though the CF₃ groups ($E_s' = 0.78$) are smaller and presumably less polarizable.²⁶ This suggested that the fluorine-containing substituents have additional stabilizing effects that are stronger than simple London dispersion interactions as observed with **L2** and **L3**. The origin for this significant and unexpected rate increase for **L4** was revealed by computational investigations as detailed below.

3.1.2. Computational Analysis of the Origin of Reactivity with Symmetric SEGPHOS Derivatives.—The preliminary experimental studies revealed promising results with the CF₃-SEGPHOS **L4** derivative. However, it was unclear what further modifications could lead to additional reactivity enhancement.^{19,27} Although successful predictions of new transition metal catalysts from computational results alone are still rare,²⁸ several examples have recently been described wherein a combination of computational and experimental evaluations has led to the discovery of catalysts with improved reactivity and selectivity.^{19,21} Such synergetic efforts effectively utilize the predictive power of computation, while the experimental verification helps resolve the uncertainty of calculated energies and issues that cannot be readily addressed by computations alone, such as catalyst decomposition.²⁹

3.1.2.1 Computational Methods: Geometry optimizations and single-point energy calculations were carried out using Gaussian 09.³⁰ Geometries of intermediates and transition states were optimized using the B3LYP functional³¹ with a mixed basis set of SDD for Cu and 6–31G(d) for other atoms in the gas phase. Vibrational frequency calculations were performed for all of the stationary points to confirm if each optimized structure is a local minimum or a transition state structure. Truhlar's quasi-harmonic corrections³² were applied for entropy calculations using 100 cm⁻¹ as the frequency cut-off.

Solvation energy corrections were calculated in THF solvent with the CPCM continuum solvation model³³ based on the gas-phase optimized geometries. The ω B97X-D functional³⁴ with a mixed basis set of SDD for Cu and 6-311+G(d,p) for other atoms was used for solvation single-point energy calculations. The computed gas-phase activation energy (E^\ddagger) was dissected using the following ligand-substrate interaction model analysis.³⁵

$$\Delta E^\ddagger = \Delta E_{\text{dist}} + \Delta E_{\text{int-bond}} + \Delta E_{\text{int-space}} \quad \text{eq.1}$$

The distortion energy (E_{dist})³⁵ is the sum of the energies required to distort the LCuH catalyst and the substrate into their transition state geometries. $E_{\text{int-space}}$ was calculated from the interaction energy of a supramolecular complex of the phosphine ligand and the olefin substrate at the transition state geometry but in the absence of the CuH moiety ($E_{\text{int-space}} = E_{\text{lig+sub}} - E_{\text{lig}} - E_{\text{sub}}$). Then, the through bond interaction was calculated from $E_{\text{int-bond}} = E^\ddagger - E_{\text{dist}} - E_{\text{int-space}}$. The E_{dist} and $E_{\text{int-space}}$ were both calculated using the ω B97X-D functional with the SDD basis set for Cu and 6-311+G(d,p) for other atoms. The ω B97X-D functional was chosen because it has been shown to accurately describe non-covalent interactions,³⁶ which we expected to be important in this system. The computed free energy barriers using this method provided very good agreement with the experimental reaction rate constants (see SI for details and comparison with results from other functionals and solvation models). The through-space interaction energy ($E_{\text{int-space}}$) between the ligand and the substrate is further dissected according to the following equation:

$$\Delta E_{\text{int-space}} = \Delta E_{\text{Pauli}} + \Delta E_{\text{elstat}} + \Delta E_{\text{pol}} + \Delta E_{\text{ct}} + \Delta E_{\text{disp}} \quad \text{eq. 2}$$

In accordance with our previous study, the dispersion energy component (E_{disp}) was obtained from the difference of interaction energies calculated using MP2 and HF. The MP2 calculations were performed with Q-Chem 5.0 using the SOS(MI)-MP2 method in combination with the dual-basis set approach utilizing the db-cc-pVTZ basis set.³⁷ The E_{Pauli} , E_{elstat} , E_{disp} , E_{pol} , and E_{ct} terms in eq 2 were calculated using the second-generation energy decomposition analysis based on absolutely localized molecular orbitals³⁸ (ALMO-EDA) method implemented in Q-Chem 5.0.³⁹ The second generation ALMO-EDA provides further decomposition of the Pauli and electrostatic interaction (E_{rep}) term into Pauli repulsion (E_{Pauli}) and electrostatic (E_{elstat}) energies, which is important in the analysis of through-space electrostatic interactions with the fluorinated ligands. To avoid double counting of dispersion, HF method with the 6-311G(d,p) basis set was employed in the energy decomposition analysis (EDA) calculations.

3.1.2.2. Computational Analysis of Symmetric-SEGPHOS Ligands.: In order to fully understand the underlying principles and interactions that lead to the enhanced rate, an in-depth computational analysis was performed to study the origin of the different hydroamination reactivities between the DTBM-SEGPHOS L2 and CF₃-SEGPHOS L4-supported CuH catalysts.

The activation energies of the rate-determining hydrocupration transition states were computed using propene (**4**) as the model substrate with the method outlined above (Table 1). The computed barrier of hydrocupration with the CF₃-SEGPPOS **L4**CuH complex was in good agreement with the experimentally observed rate increase with **L4** compared to DTBM-SEGPPOS **L2**CuH ($G_{\text{comp}}^{\ddagger} = 1.5$ kcal/mol vs $G_{\text{exp}}^{\ddagger} = 1.1$ kcal/mol). In order to quantify the different factors that lead to the improved reactivity, the ligand-substrate interaction model analysis was employed to dissect the overall hydrocupration activation energies (Eqs. 1 and 2, see Computational Methods for details). Energy-decomposition analysis of the hydrocupration transition state with **L4**CuH revealed that the increase in the reaction rate was due to significantly stronger through-bond interactions ($E_{\text{int-bond}}$) resulting in an extra 2.3 kcal/mol stabilization of **TS-4** compared to the DTBM-SEGPPOS-bound **TS-2**. This is because of the electron-withdrawing nature of the CF₃-substituents which consequently results in enhanced Lewis acidity of the CuH catalyst and more favorable binding of the olefin substrate (see SI for details). While the through-space interaction energies ($E_{\text{int-space}}$) are comparable in **TS-2** and **TS-4**, the origins are different. Using the second-generation ALMO-EDA methods, the $E_{\text{int-space}}$ term was further dissected into its individual energy components (Eq. 2). While **TS-2** is stabilized by stronger attractive London dispersion ($E_{\text{disp}} = -13.3$ kcal/mol for **TS-2** compared to -10.7 kcal/mol for **TS-4**), electrostatic interactions are more favorable in **TS-4** ($E_{\text{elstat}} = 0.3$ kcal/mol for **TS-2** compared to -1.5 kcal/mol for **TS-4**). The optimized geometry of **TS-4** revealed multiple C-F...H-C contacts, which are responsible for the through-space electrostatic interactions between **L4** and the olefin substrate thereby lowering E^{\ddagger} (Figure 4).

Although the use of CF₃-SEGPPOS **L4** leads to a relatively moderate increase of reactivity, the computational analysis suggested types of modifications that might result in a more effective ligand. Considering that the CF₃-SEGPPOS **L4** ligated LCuH complex has weakened dispersion interactions when compared to the **L2**CuH complex, we hypothesized that the installation of a larger perfluorinated substituent would be beneficial. Since the *i*-C₃F₇ group is sterically more demanding than CF₃, we assumed that it should increase stabilizing London dispersion, while maintaining the favorable through-space electrostatic attractions and through-bond electronic effects.

Indeed, the calculated hydrocupration transition state **TS-5** indicated that the use of *i*-C₃F₇-SEGPPOS **L5** as the ligand led to an additional 1.5 kcal/mol lower activation energy compared to the hydrocupration with **L4**CuH (Table 1).

The ligand-substrate interaction model analysis validated our hypothesis, as the E_{dist} and $E_{\text{int-bond}}$ terms of **TS-5** remained largely unchanged when compared to **TS-4**. Meanwhile, the through-space interaction of **TS-5** was 1.7 kcal/mol more stabilizing. Further dissection of the through-space interactions revealed that the primary reason for the increased reactivity was due to the increased London-dispersion interactions (E_{disp}) in **TS-5**. To validate this computational prediction, we needed to experimentally measure the reactivity of *i*-C₃F₇-SEGPPOS-supported CuH catalyst **L5**CuH.

3.1.4. Synthesis and Kinetic Analysis of Hydroamination with the Symmetric *i*-C₃F₇-SEGPPOS Ligand.—

Informed by the computational predictions described above,

we set out to synthesize ligand **L5**. Adopting a closely related report by Yu, we were able to prepare **L5** from dibromide **5** and *bis*-(3,5-*i*-C₃F₇-C₆H₃)₂PBr (**6**) in a single step (Scheme 2a).⁴⁰

When **L5** was employed with the standard catalytic conditions, *vide supra*, the formation of hydroamination product **3** was observed to be 61 times faster than with **L2**, indicating that increased London dispersion interactions were indeed facilitating the hydrocupration event. However, only a short burst of reactivity was observed under the reaction conditions employing **L5**. This suggests that the **L5**CuH complex, although an active catalyst, was not stable under the reaction conditions (Figure 6, red curve).⁴¹ This catalyst decomposition is most likely the consequence of the diminished Lewis basicity of the phosphorus atoms in **L5**, due to the electron-withdrawing nature of the *i*-C₃F₇ substituents which results in weaker binding to the copper center. In order to exhibit both high reactivity and stability, the Lewis acidity of the copper center needed to be finely tuned.

3.1.5. Hybrid-SEGPPOS Ligands—To harness the increased reactivity that we observed using the *i*-C₃F₇ substituents without sacrificing the stability of the resulting complex, we had two options: either to synthesize and test various new derivatives with different substituents, in order to find a suitable ligand that provides a catalyst system that combines high activity and stability, or exchange one *P*-aryl₂ substituent for a more electron-donating group in order to stabilize the resulting copper complex. To avoid significant structural changes at the 3- and 5-positions of the aryl groups, we reasoned that the merger of DTBM-**L2** and *i*-C₃F₇-**L5**, the ligands with higher catalyst stability and reactivity, might result in the perfect balance of their respective beneficial interactions. This hypothesis found further support in examining the transition-state structure **TS-5**, in which the improved through-space ligand-substrate interactions primarily arise from the C–F...H–C interactions in the 1st and 4th quadrants (Figure 5). The *i*-C₃F₇ groups in the 2nd and 3rd quadrants are further away from the substrate, and thus are less significant in promoting the hydrocupration step. Therefore, exchanging the *P*-aryl₂ groups in the 2nd and 3rd quadrants was not expected to significantly impact the enhanced reactivity gained from the *i*-C₃F₇ moieties.

3.1.5.1 Computational Studies of Hydrocupration with Hybrid-SEGPPOS

Ligands: The computational investigations showed that the hydrocupration barrier for the hybrid SEGPPOS derivative **L6**CuH was similar to that of the symmetric derivative **L5**CuH (see Table 1). In the lowest energy transition state structure with **L6** (**TS-6**, Figure 5), the methyl group on propene (**4**) prefers to be placed in the *i*-C₃F₇-occupied 1st quadrant, rather than the DTBM-occupied 3rd quadrant (**TS-6a**, Figure 5), indicating the C–F...H–C non-covalent interactions with the *i*-C₃F₇ group are more favorable than the C–H...H–C interactions with the *t*-Bu group. Further energy decomposition analysis showed similar through-space interaction energies ($E_{\text{int-space}}$) in **TS-6** and **TS-5** (Table 1). While electrostatic interactions in **TS-6** were slightly decreased relative to those in **TS-5**, London dispersion interactions were increased as a result of the larger *t*-butyl substituents in the 2nd and 3rd quadrants of **TS-6**. This finding indicated, that a comparable energy barrier of hydrocupration might be obtained from **L6**CuH.

3.1.5.2 Synthesis of Hybrid-SEGPHOS Ligands: To verify our hypothesis, a practical synthetic sequence had to be developed to prepare this hybrid ligand. After extensive experimental effort, a modular three-step sequence was established (Scheme 2b). The installation of the *bis*-(3,5-CF₃-C₆H₃)₂P subunit was achieved by trapping mono-magnesiated **5** with freshly prepared *bis*-(3,5-*i*-C₃F₇-C₆H₃)₂PBr (**6**). After, the introduction of the DTBM-P(O) moiety, *via* a palladium catalyzed cross-coupling reaction with DTBM phosphine oxide **7**, and subsequent reduction, **L6** was obtained in 26% yield over 3 steps.⁴²

3.1.5.3 Kinetic Analysis of Hybrid-SEGPHOS Ligands: Following our standard kinetic protocol, **L6** was employed with our usual catalytic conditions and the formation of hydroamination product **3** was found to be 62 times faster than that when using **L2**, indicating that the rate enhancement observed with the symmetric **L5CuH** complex was maintained (Figure 6, black curve). We also noted that no detectable catalyst decomposition was observed with **L6** under the reaction conditions, validating our hypothesis that the hybrid system could maintain stability without sacrificing reactivity.³⁸

3.1.6. Demonstration of Hybrid-SEGPHOS Ligand L6 under Preparative Conditions.—In order for this newly developed ligand to be useful in a synthetic context, the observed rate increase would need to be maintained at preparatively relevant scales and on substrates bearing functional groups. After slight optimization of the reaction conditions, the scope of olefins was established using hydroxylamine ester **2** as the amine source (Table 2). The hydroamination of terminal olefins that contained various functional groups were surveyed at room temperature. Epoxide **8**, ester **9**, silyl ether **10**, and ketal **11** all provided the desired tertiary amine product in excellent yield. Moreover, substrates that contained a variety of heterocycles, such as piperazine **12**, morpholine **13**, and thiophene **14** also underwent smooth hydroamination at room temperature. Stronger Lewis bases found in heterocyclic compounds like indole **15**, benzothiazole **16**, pyrimidine **17**, and in quinolines **18** and **19** slightly inhibited the reaction, and thus their reactions required slightly elevated temperatures (40 °C) to reach full conversion within 3 hours. To compare our new catalyst to the current state-of-the-art catalyst, **L2**, epoxide **8** and ester **9** were subjected to these reaction conditions employing DTBM-**L2** as the ligand.⁴³ Diminished yields of 17 and 29% were observed compared to 89 and 94% with **L6**, respectively. This demonstrates that the rate enhancement using this catalyst system is maintained under preparative reaction conditions.

CONCLUSION

This study demonstrates how the combination of mechanistic insights, computational prediction, and experimental verification can successfully benefit ligand development. Using this synergistic approach we were able to discover a new hybrid ligand **L6** that is capable of promoting the *anti*-Markovnikov hydroamination of unactivated, terminal olefins with a 62 fold rate increase compared to DTBM-SEGPHOS **L2**. By employing energy decomposition analysis methods, we were able to deconvolute each individual energy contributions of the steric, electronic, and dispersion effects that comprise the hydrocupration barrier. During the course of our investigation we identified that in addition to London dispersion, both

electrostatic C–F...H–C non-covalent interactions and inductive effects of the *i*-C₃F₇ substituents are capable of lowering the energy barrier for hydrocupration even further. Ultimately, the merger of both DTBM and *i*-C₃F₇ substituents was key to success in designing **L6** with balanced stability and reactivity. Furthermore, a modular and robust synthetic sequence to access these novel hybrid ligand structures was devised, that allowed for its gram-scale synthesis. In addition, the effectiveness of the catalyst system employing **L6** was proven under preparative conditions. We anticipate that this rational ligand design approach can be utilized in other catalytic systems providing accelerated reaction development.

Supplementary Material

Refer to Web version on PubMed Central for supplementary material.

ACKNOWLEDGMENT

This material is based upon work supported by the NIH Postdoctoral Fellowship Program under Grant No. 1F32GM125163 (A.A.T.), Leopoldina - National Academy of Science under Grant No. LPDS2017-08 (K.S.) and the NIH (Grant No. GM122483 and R35GM128779). Any opinions, findings, conclusions, or recommendations expressed in this material are those of the authors and do not necessarily reflect the views of the NIH. We are grateful to Drs. Peter Müller and Charlene Tsay for crystallographic analysis, and we acknowledge Richard Liu and Drs. Christine Nguyen and Scott McCann for assistance in the preparation of this manuscript. Calculations were performed at the Center for Research Computing at the University of Pittsburgh and the Extreme Science and Engineering Discovery Environment (XSEDE) supported by the NSF.

REFERENCES

- (1). Zhu S; Niljianskul N; Buchwald SL J. Am. Chem. Soc. 2013, 135, 15746–15749. [PubMed: 24106781]
- (2). Miki Y; Hirano K; Satoh T; Miura M Angew. Chem. Int. Ed. 2013, 52, 10830–10834.
- (3). (a) Pirnot MT; Wang YM; Buchwald SL Angew. Chem. Int. Ed. 2016, 55, 48–57. (b) Zhu S; Buchwald SL J. Am. Chem. Soc. 2014, 136, 15913–15916. [PubMed: 25339089]
- (4). Niljianskul N; Zhu S; Buchwald SL Angew. Chem. Int. Ed. 2015, 54, 1638–1641.
- (5). (a) Shi SL; Buchwald SL Nat Chem. 2015, 7, 38–44. [PubMed: 25515888] (b) Severin R; Doye S Chem. Soc. Rev. 2007, 36, 1407–1420. [PubMed: 17660874]
- (6). (a) Friis SD; Pirnot MT; Dupuis LN; Buchwald SL Angew. Chem. Int. 2017, 56, 7242–7246. (b) Yang Y; Shi SL; Niu D; Liu P; Buchwald SL Science. 2015, 349, 62–66. [PubMed: 26138973]
- (7). For representative examples of other methods of hydroamination, see: (a) Musacchio AJ; Lainhart BC; Zhang X; Naguib SG; Sherwood TC; Knowles RR Science. 2017, 355, 727–750. [PubMed: 28209894] (b) Ensign SC; Vanable EP; Kortman GD; Weir LJ; Hull KL J. Am. Chem. Soc. 2015, 137, 13748–13751. [PubMed: 26456593] (c) Nguyen TM; Manohar N; Nicewicz DA; Angew. Chem. Int. 2014, 53, 6198–6201. (d) Banerjee D; Junge K; Beller M Org. Chem. Front. 2014, 1, 368–372. (e) Rucker RP; Whittaker AM; Dang H; Lalic GJ Am. Chem. Soc. 2012, 134, 6571–6574. (f) Shapiro ND; Rauniyar V; Hamilton GL; Wu J; Toste D Nature, 2011, 470, 245–249. [PubMed: 21307938] (g) Seayad J; Tillack A; Hartung CG; Beller M Adv. Synth. Catal. 2002, 344, 795–813. (h) Schlummer B; Hartwig JF Org. Lett. 2002, 1471–1474. [PubMed: 11975606]
- (8). (a) Bernoud E; Lepori C; Mellah M; Schulz E; Hannedouche J Catal. Sci. Technol. 2015, 5, 2017–2037. (b) Hultsch KC Org. Biomol. Chem. 2005, 3, 1819–1824. [PubMed: 15889160]
- (9). Dewick PM Medicinal natural products: a biosynthetic approach, 3rd edition ed., Wiley, Chichester, West Sussex, England; New York, NY, USA, 2009.
- (10). For reviews of methods for the synthesis of amines, see: (a) Baxter EW; Reitz AB Organic Reactions 2002, 59, 1–741. (b) Chiral Amine Synthesis; Nugent TC, Ed.; Wiley-VCH: Weinheim, 2010.

- (11). Liu RY; Buchwald SL *Org. Synth.* 2018, 95, 80–96. [PubMed: 30287975]
- (12). Bandar JS; Pirnot MT; Buchwald SL *J. Am. Chem. Soc.* 2015, 137, 14812–14818. [PubMed: 26522837]
- (13). For representative examples of aminoboration, see:(a) Xi Y; Hartwig JF *J. Am. Chem. Soc.* 2017, 139, 12758–12772. [PubMed: 28787137] (b) Lee J; Radomkit S; Torker S; Pozo JD; Hoveyda AH *Nat. Chem.* 2017, 10, 99–108. [PubMed: 29256506]
- (14). (a) Lu G; Liu RY; Yang Y; Fang C; Lambrecht DS; Buchwald SL; Liu PJ *Am. Chem. Soc.* 2017, 139, 16548–16555.(b) Tobisch S *Chem. Sci.* 2017, 8, 4410–4423. [PubMed: 28660063]
- (15). We propose a mechanism that is consistent with all of the current data but we cannot exclude the possibility that the C-N bond forming step occurs through an outersphere process.
- (16). Echeverria J; Aullon G; Danovich D; Shaik S; Alvarez S *Nature Chem.* 2011, 3, 323–330. [PubMed: 21430693]
- (17). (a) Neel AJ; Hilton MJ; Sigman MS; Toste FD *Nature* 2017, 543, 637–646. [PubMed: 28358089] (b) Wagner JP; Schreiner PR *Angew. Chem., Int. Ed.* 2015, 54, 12274–12296.
- (18). (a) Xu X; Liu P; Lesser A; Sirois LE; Wender PA; Houk KN *J. Am. Chem. Soc.* 2012, 134, 11012–11025. [PubMed: 22668243] (b) Wolters LP; Koekkoek R; Bickelhaupt FM *ACS Catal.* 2015, 5, 5766–5775.(c) Lyngvi E; Sanhueza IA; Schoenebeck F *Organometallics* 2015, 34, 805–812.(d) Meyer TH; Liu W; Feldt M; Wuttke A; Mata RA; Ackermann L *Chem. - Eur. J.* 2017, 23, 5443–5447. [PubMed: 28317205] (e) Cundari TR; Jacobs BP; MacMillan SN; Wolczanski PT *Dalton Trans.* 2018, 47, 6025–6030. [PubMed: 29687794]
- (19). (a) Hale LVA; Szymczak NK *ACS Catal.* 2018, 8, 6446–6461.(b) Chattopadhyay B; Dannatt JE; Sanctis ILAD; Gore KA; Maleczka RE; Singleton DA; Smith MR *J. Am. Chem. Soc.* 2017, 139, 7864–7871. [PubMed: 28453268] (c) Davis HJ; Mihai MT; Phipps RJ *J. Am. Chem. Soc.* 2016, 138, 12759–12762 [PubMed: 27626468] (d) Kuninobu Y; Ida H; Nishi M; Kanai M *Nat. Chem.* 2015, 7, 712–717. [PubMed: 26291942]
- (20). (a) Kui SCF; Zhu N; Chan MCW *Angew. Chem. Int. Ed.* 2003, 42, 1628–1632.(b) Mitani M; Mohri J; Yoshida Y; Saito J; Ishii S; Tsuru K; Matsui S; Furuyama R; Nakano T; Tanaka H; Kojoh S; Matsugi T; Kashiwa N; Fujia TJ *Am. Chem. Soc.* 2002, 124, 13, 3327–3336.
- (21). (a) Luo SX; Engle KM; Dong X; Heji A; Takase MK; Henling LM; Liu P; Houk KN; Grubbs RH *ACS Catal.* 2018, 8, 4600–4611.(b) Burrows LC; Jesikiewicz LT; Lu G; Geib SJ; Liu P; Brummond KM *J. Am. Chem. Soc.* 2017, 139, 15022–15032. [PubMed: 29022341]
- (22). (a) Straker RN; Mekareeya A; Paton RS; Anderson EA *Nat. Commun.* 2016, 7, 10109–10118. [PubMed: 26728968] (b) Kwon D; Fuller JT; Kilgore UJ; Sydora OL; Bischof SM; Ess DH *ACS Catal.* 2018, 8, 1138–1142.(c) Nielsen MC; Bonney KJ; Schoenebeck F *Angew. Chem. Int. Ed.* 2014, 53, 5903–5906.(d) Bernales V; League AB; Li Z; Schweitzer NM; Peters AW; Carlson RK; Hupp JT; Cramer CJ; Farha OK; Gagliardi LJ *Phys. Chem. C* 2016, 120, 23576–23583.(e) Sinha I; Lee Y; Bae C; Tussupbayev S; Lee Y; Seo M; Kim J; Baik M; Lee Y; Kim H *Catal. Sci. Technol.* 2017, 7, 4375–4387.(f) Wang Y; Wang J; Su J; Huang F; Jiao L; Liang Y; Yang D; Zhang S; Wender PA; Yu Z-XJ *Am. Chem. Soc.* 2007, 129, 10060–10061.(g) Occhipinti G; Koudriavtsev V; Törnroos KW; Jensen VR *Dalton Trans.* 2014, 43, 11106–11117. [PubMed: 24788021]
- (23). Ligands L2 and L3 were prepared according to: Sevov CS; Hartwig JF *J. Am. Chem. Soc.* 2014, 136, 10625–10631. [PubMed: 25032781]
- (24). The hydrocupration event has been shown previously to be the rate determining step for terminal olefins with DTBM-SEGPHOS, see ref 13. Additionally, ligand L6 exhibited clean first order profiles along with a first order dependence on the olefin substrate, see supplementary material.
- (25). Macphee JA; Panaye A; Dubois JE *Tetrahedron*, 1978, 34, 2253–3562.
- (26). O'Hagan D *Chem. Soc. Rev.* 2008, 37, 308–319. [PubMed: 18197347]
- (27). Iwamoto H; Imamoto T; Ito H *Nat. Commun.* 2018, 9, 2290. [PubMed: 29895938]
- (28). (a) Guan Y; Wheeler SE *Angew. Chem. Int. Ed.* 2017, 56, 9101–9105.(b) Poree C; Schoenebeck F *Acc. Chem. Res.* 2017, 50, 605–608. [PubMed: 28945392]
- (29). Sperger T; Sanhueza IA; Schoenebeck F *Acc. Chem. Res.* 2016, 49, 1311–1319. [PubMed: 27171796]

- (30). Frisch MJ; Trucks GW; Schlegel HB; Scuseria GE; Robb MA; Cheeseman JR; Scalmani G; Barone V; Mennucci B; Petersson GA; Nakatsuji H; Caricato M; Li X; Hratchian HP; Izmaylov AF; Bloino J; Zheng G; Sonnenberg JL; Hada M; Ehara M; Toyota K; Fukuda R; Hasegawa J; Ishida M; Nakajima T; Honda Y; Kitao O; Nakai H; Vreven T; Montgomery JA Jr.; Peralta JE; Ogliaro F; Bearpark M; Heyd JJ; Brothers E; Kudin KN; Staroverov VN; Kobayashi R; Normand J; Raghavachari K; Rendell A; Burant JC; Iyengar SS; Tomasi J; Cossi M; Rega N; Millam NJ; Klene M; Knox JE; Cross JB; Bakken V; Adamo C; Jaramillo J; Gomperts R; Stratmann RE; Yazyev O; Austin AJ; Cammi R; Pomelli C; Ochterski JW; Martin RL; Morokuma K; Zakrzewski VG; Voth GA; Salvador P; Dannenberg JJ; Dapprich S; Daniels AD; Farkas Ö; Foresman JB; Ortiz JV; Cioslowski J; Fox DJ Gaussian 09, Revision D.01; Gaussian, Inc: Wallingford, CT, 2009.
- (31). (a) Lee C; Yang W; Parr RG Phys. Rev. B 1988, 37, 785;(b) Becke AD J. Chem. Phys. 1993, 98, 5648–5652.
- (32). Ribeiro RF; Marenich AV; Cramer CJ; Truhlar DG J. Phys. Chem. B 2011, 115, 14556–14562. [PubMed: 21875126]
- (33). (a) Cossi M; Rega N; Scalmani G; Barone VJ Comp. Chem, 2003, 24, 669–681.(b) Barone V; Cossi MJ Phys. Chem. A, 1998, 102, 1995–2001.
- (34). Chai JD; Head-Gordon M Phys. Chem. Chem. Phys, 2008, 10, 6615–6620. [PubMed: 18989472]
- (35). Bickelhaupt FM; Houk KN Angew. Chem., Int. Ed. 2017, 56, 10070–10086.
- (36). (a) Peverati R; Truhlar DG J. Phys. Chem. Lett, 2011, 21, 2810–2817.(b) Burns LA; Vázquez-Mayagoitia A; Sumpter BG; Sherrill CD J. Chem. Phys. 2011, 134, 084107. [PubMed: 21361527]
- (37). (a) Distasio RA Jr., ; Head-Gordon M Mol. Phys. 2007, 105, 1073–1083.(b) Steele RP; DiStasio RA; Shao Y; Kong J; Head-Gordon MJ Chem. Phys. 2006, 125, 074108.
- (38). (a) Horn PR; Head-Gordon MJ Chem. Phys. 2016, 144, 084118.(b) Horn PR; Mao Y; Head-Gordon MJ Chem. Phys. 2016, 144, 114107.(c) Horn PR; Mao Y; Head-Gordon M Phys. Chem. Chem. Phys, 2016, 18, 23067–23079. [PubMed: 27492057]
- (39). Shao Y; Gan Z; Epifanovsky E; Gilbert ATB; Wormit M; Kussmann J; Lange AW; Behn A; Deng J; Feng X; Ghosh D; Goldey M; Horn PR; Jacobson LD; Kaliman I; Khaliullin RZ; Kus T; Landau A; Liu J; Proynov EI; Rhee YM; Richard RM; Rohrdanz MA; Steele RP; Sundstrom EJ; Woodcock HL; Zimmerman PM; Zuev D; Albrecht B; Alguire E; Austin B; Beran GJO; Bernard YA; Berquist E; Brandhorst K; Bravaya KB; Brown ST; Casanova D; Chang C-M; Chen Y; Chien SH; Closser KD; Crittenden DL; Diedenhofen M; DiStasio RA; Do H; Dutoi AD; Edgar RG; Fatehi S; Fusti-Molnar L; Ghysels A; Golubeva-Zadorozhnaya A; Gomes J; Hanson-Heine MWD; Harbach PHP; Hauser AW; Hohenstein EG; Holden ZC; Jagau T-C; Ji H; Kaduk B; Khistyayev K; Kim J; Kim J; King RA; Klunzinger P; Kosenkov D; Kowalczyk T; Krauter CM; Lao KU; Laurent AD; Lawler KV; Levchenko SV; Lin CY; Liu F; Livshits E; Lochan RC; Luenser A; Manohar P; Manzer SF; Mao S-P; Mardirossian N; Marenich AV; Maurer SA; Mayhall NJ; Neuscammen E; Oana CM; Olivares-Amaya R; O'Neill DP; Parkhill JA; Perrine TM; Peverati R; Prociuk A; Rehn DR; Rosta E; Russ NJ; Sharada SM; Sharma S; Small DW; Sodt A Mol. Phys. 2015, 113, 184–215
- (40). The corresponding diarylchlorophosphine resulted in no product formation; see: Liu L; Wu HC; Yu JQ; Chem. Eur. J. 2011, 17, 10828–10831. [PubMed: 21853488]
- (41). Colloidal copper was observed after a few minutes along with the observation of unbound L5.
- (42). The structure of L6 was additionally validated by single crystal X-ray analysis (see supplementary information for details).
- (43). The reactions of substrates incorporating an imidazole unit resulted in no product formation, presumably due to the imidazole's Lewis basicity.

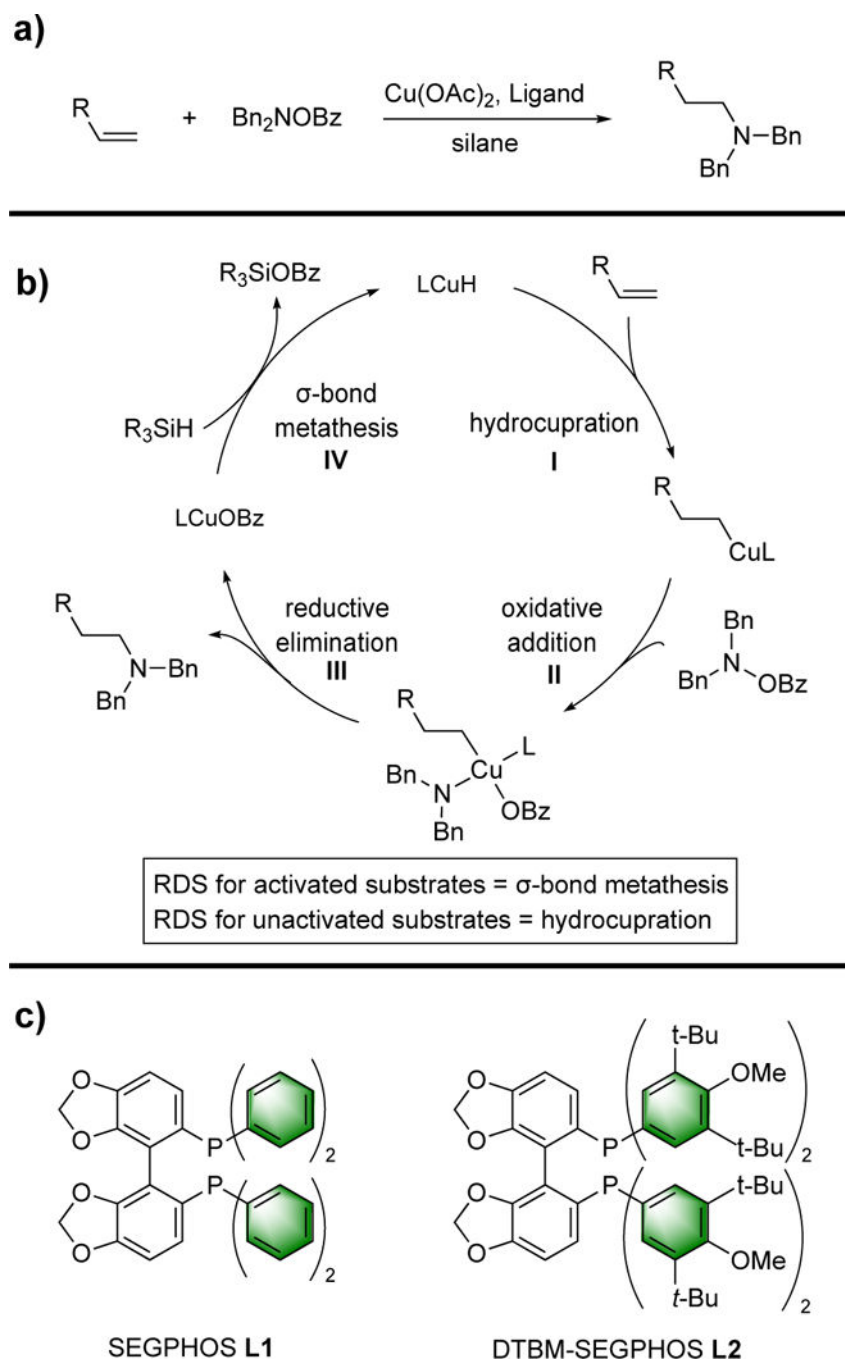
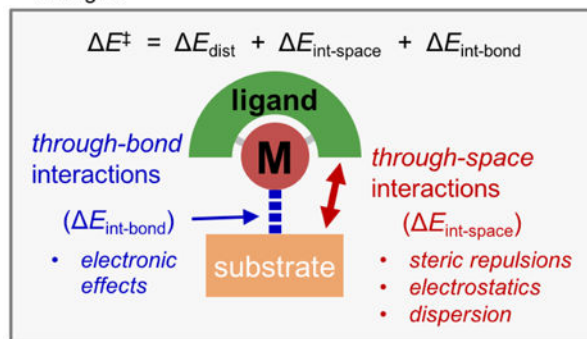


Figure 1.
 a) LCuH-catalyzed *anti*-Markovnikov hydroamination reaction. b) Proposed catalytic cycle for LCuH-catalyzed *anti*-Markovnikov hydroamination reaction. c) SEGPHOS **L1** and DTBM-SEGPHOS **L2** ligands.

a) Ligand-substrate interaction model to dissect activation energies



b) Ligand-substrate dispersion interactions in hydrocupration transition state

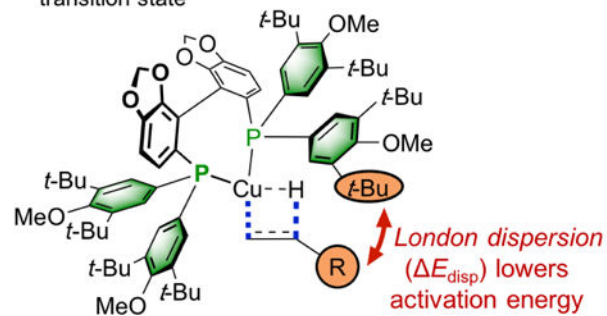


Figure 2.

a) Ligand-substrate interaction model to study the origin of reactivity in hydrocupration. b) London dispersion interactions lowering the hydrocupration barrier for L_2CuH .

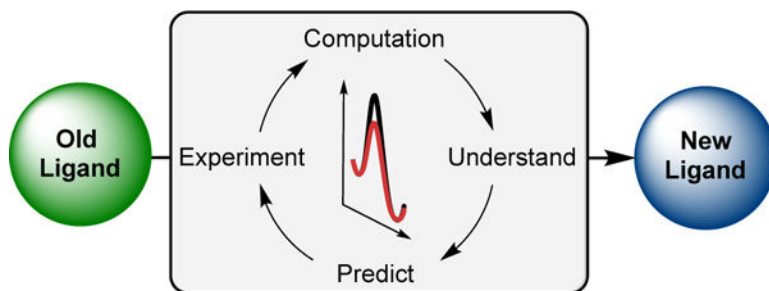


Figure 3.
Project outline.

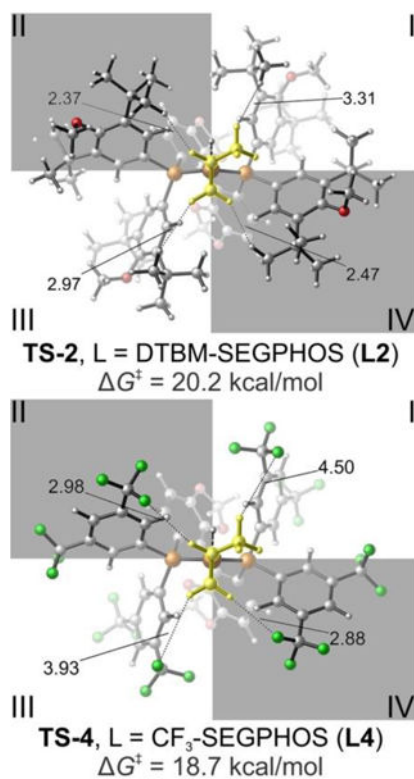


Figure 4. Optimized geometries of hydrocupration transition states with the DTBM-SEGPHOS (**TS-2**) and CF₃-SEGPHOS ligands (**TS-4**). Distances are in Ångström [Å].

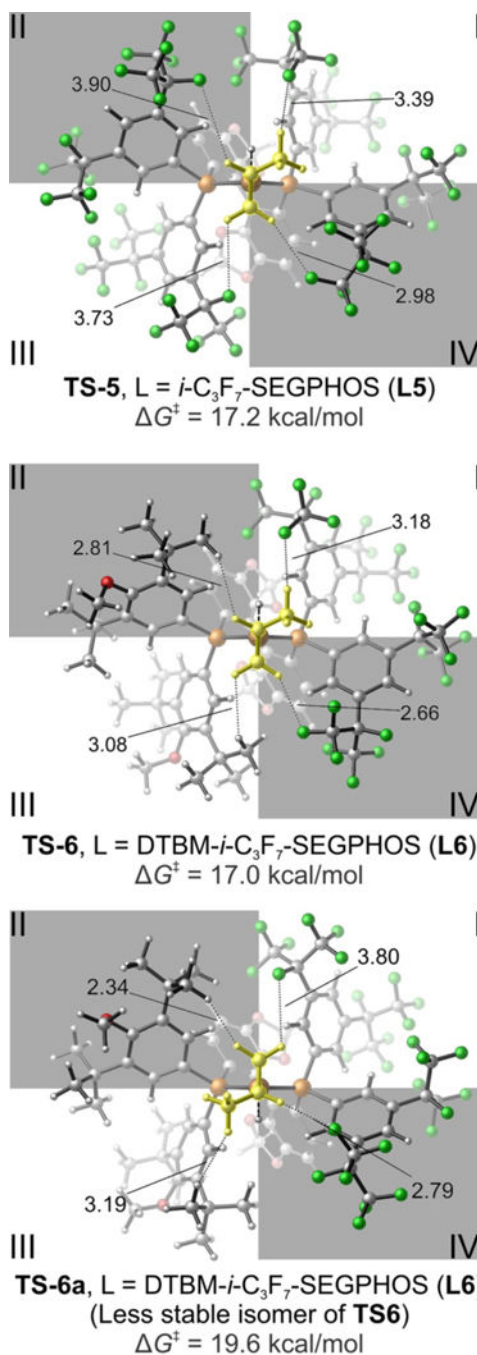


Figure 5. Optimized geometries of hydrocupration transition states with the *i*-C₃F₇-SEGP_{HOS} (**TS-5**) and the hybrid DTBM-*i*-C₃F₇-SEGP_{HOS} ligand (**TS-6** and **TS-6a**). Distances are reported in Ångström [Å].

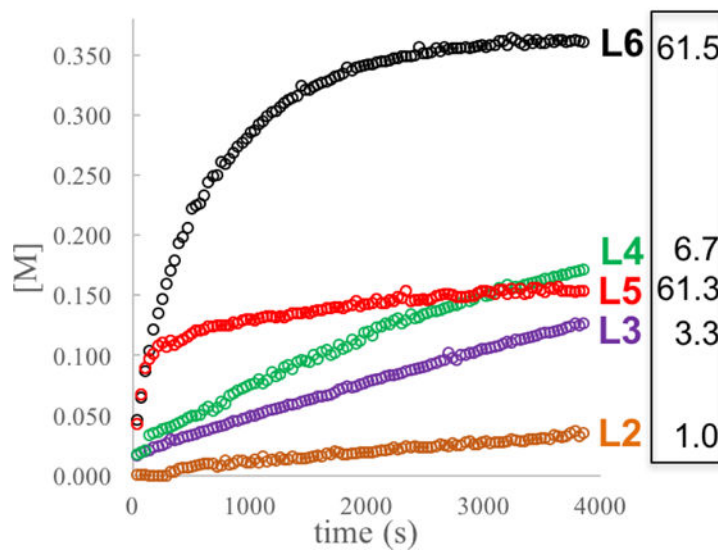
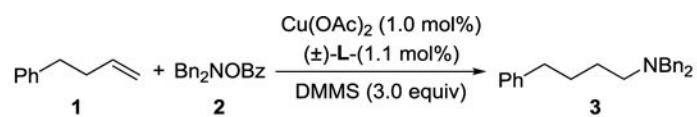
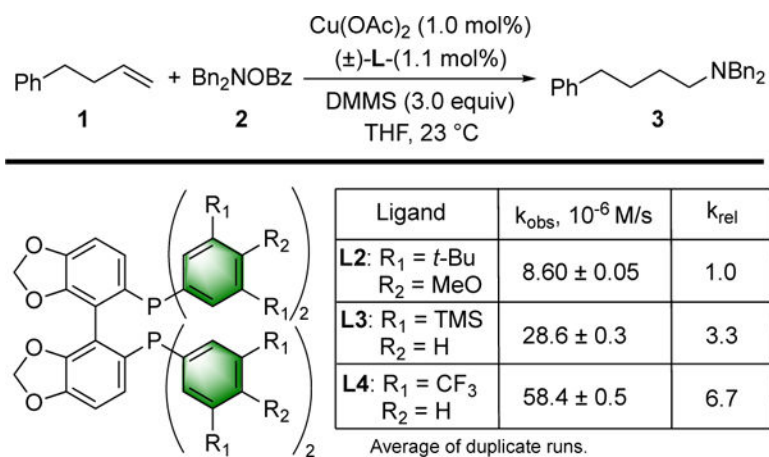
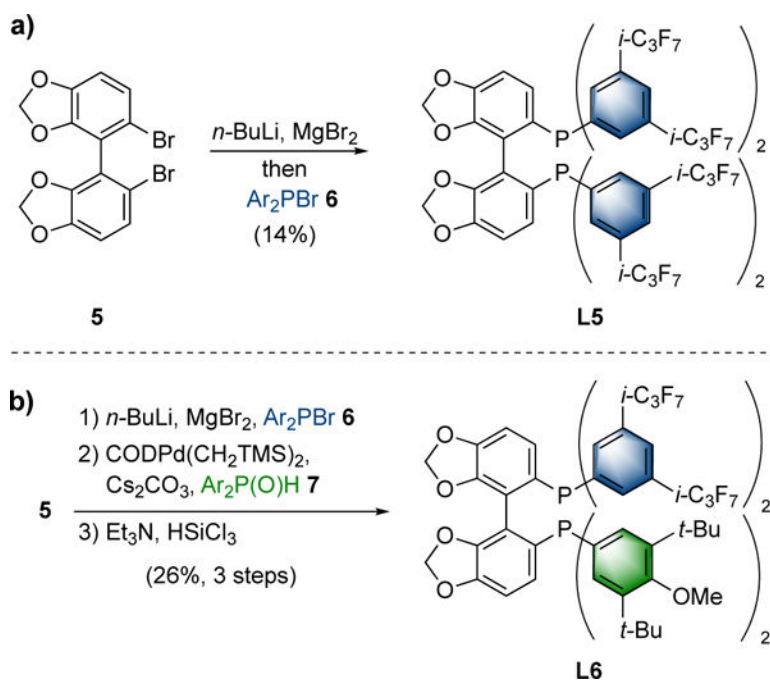


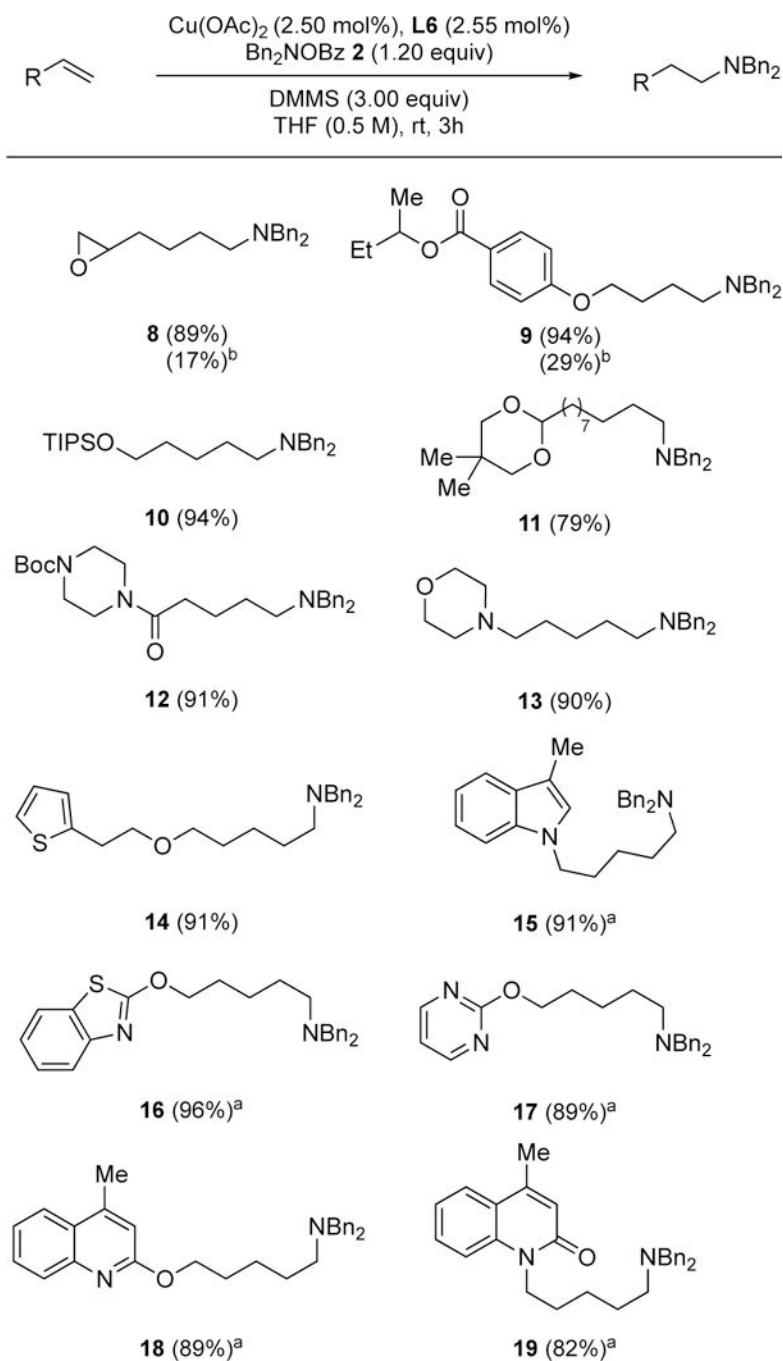
Figure 6. Combined data for the formation of amination product **3** (see, supplementary information for details).

**Scheme 1.**

Initial kinetic analysis for symmetric ligands **L2**, **L3** and **L4**.

**Scheme 2.**

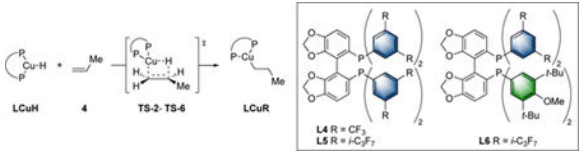
Synthesis of SEGPHOS derivatives **L5** and **L6** (see supplementary information for details).

**Scheme 3.**

Isolated yields are reported as the average of two runs. Standard reaction conditions: terminal olefin (0.50 mmol), Bn_2NOBz (**2**) (0.60 mmol), Cu(OAc)_2 (2.50 mol%), **L6** (2.55 mol%), DMMS (1.50 mmol), THF (1.0 mL), 23 °C, 3h. ^a40 °C. ^b DTBM-SEGPHOS was used in place of **L6** and NMR yields are provided.

Table 1.

Activation free energies of the hydrocupration transition states and energy components derived from the ligand-substrate interaction model.^a



ligand	DTBM (L2)	CF ₃ (L4)	<i>i</i> -C ₃ F ₇ (L5)	DTBM- <i>i</i> -C ₃ F ₇ (L6)
hydrocupration transition state	TS-2	TS-4	TS-5	TS-6
$G_{\text{solv}}^{\ddagger}$	20.2	18.7	17.2	17.0
E^{\ddagger}	-0.1	-1.0	-3.4	-3.0
distortion ($E_{\text{dist}}^{\ddagger}$)	28.6	29.5	28.8	27.9
through-bond interaction ($E_{\text{int-bond}}^{\ddagger}$)	-23.9	-26.2	-26.2	-25.4
through-space interaction ($E_{\text{int-space}}^{\ddagger}$)	-4.8	-4.3	-6.0	-5.6
Pauli repulsion ($E_{\text{Pauli}}^{\ddagger}$)	9.0	8.4	7.9	7.8
electrostatic ($E_{\text{elstat}}^{\ddagger}$)	0.3	-1.5	-1.2	-0.3
London dispersion ($E_{\text{disp}}^{\ddagger}$)	-13.3	-10.7	-11.9	-13.0
charge transfer (E_{ct}^{\ddagger})	-0.2	-0.2	-0.1	0.0
polarization ($E_{\text{pol}}^{\ddagger}$)	-0.6	-0.4	-0.4	-0.4
$G_{\text{comp}}^{\ddagger}$	0.0	-1.5	-3.0	-3.2
$G_{\text{exp}}^{\ddagger}$	0.0	-1.1	-2.4	-2.4

^aAll energies are reported in kcal/mol. The activation energies ($G_{\text{solv}}^{\ddagger}$ and E^{\ddagger}) are with respect to the separated CuH catalyst and propene (**4**).

$G_{\text{comp}}^{\ddagger}$ values were calculated by subtracting $G_{\text{solv}}^{\ddagger}$ -L2 from $G_{\text{solv}}^{\ddagger}$ -LX. $G_{\text{exp}}^{\ddagger}$ were derived from the experimental relative rate constants (k_{rel}).